PROCEEDINGS, Thirty-Fifth Workshop on Geothermal Reservoir Engineering
Stanford University, Stanford, California, February 1-3, 2010
SGP-TR-188

IN-SITU MULTIFUNCTION NANOSENSORS FOR FRACTURED RESERVOIR CHARACTERIZATION

Mohammed Alaskar, Morgan Ames, Roland Horne, Kewen Li, Steve Connor and Yi Cui

Department of Energy Resources Engineering, Stanford University
367 Panama Street, Stanford, CA 94305, USA
e-mail: askar@stanford.edu; mames@stanford.edu; horne@stanford.edu; kewenli@stanford.edu; stconnor@stanford.edu; yicui@stanford.edu

ABSTRACT

Acquiring specific data about the reservoir pressure and temperature, near the wellbore and far out in the formation, and correlating such information to fracture connectivity and geometry are key for the optimum energy extraction from geothermal resources. Existing fracture characterization tools and analysis approaches are inadequate, in that pressure and temperature are measured only at the wellbore. Technological advancement in nanoscience could provide a boost in the area of reservoir in-situ measurements through the concept of nanosensing.

This paper provides some details of initial experimental work done so far towards the ultimate goal of making temperature and pressure nanosensors from which a new method will be developed to predict reservoir parameters and characterize fracture networks in geothermal reservoirs. The paper addresses the feasibility of using nanomaterials as tracers in sensing the reservoir properties in-situ. Preliminary testing with the injection of various nanofluid suspensions (nanoparticles and nanowires) was carried out to investigate the viability of transporting nanomaterials through a porous medium. This is a critical step toward the development of functional nanosensors. Berea sandstone and sand-packed slim tube were used in the nanofluid injection experiments. The nanoparticles injected into Berea sandstone samples have provided a proof of concept in the use of nanoparticles as tracers. The nanoparticles were transported through the pore space of the rock and were detected in the effluent. The nanoparticles were also recovered through the 10 meter long sand-packed slim tube. Following the successful injection of spherically shaped nanoparticles, an investigation was initiated to assess the practicability of transporting wire-like nanoparticles (silver nanowires) through the pores of Berea sandstone. These nanowires serve as precursor for the injection of functional nanosensors such as pressure- and temperature-sensitive nanotracers. It was found that the silver nanowires of that particular size could not pass through the pore spaces of the core sample.

INTRODUCTION

In the development of enhanced geothermal systems, the characterization of the size, shape and conductivity of fractures is crucial. Unlike conventional geothermal systems, enhanced geothermal systems do not require natural convective hydrothermal resources, but rather can be created in a hot, dry and impermeable volume of rock. Hydraulic stimulation of fractures is the primary means of creating functional geothermal reservoirs at such sites to allow economical heat recovery. The energy extraction rate is significantly dependent on the creation of fractured area within the targeted hot rock volume. Mapping fractured area is of equal importance. However, existing fracture characterization tools and analysis approaches are insufficient. Pressure and temperature measurements are obtained only at the wellbore or a couple of feet around it, and it is not possible to determine the conditions out in the reservoir. Currently, there are no effective means to measure such properties far in the rock formations as a way to determine the efficacy of the fracture treatment. Thus, the objectives of this research are to provide a new tool (nanosensors) and to develop reservoir engineering approaches to estimate reservoir parameters and characterize fracture networks based on the measurements from these tools. Natural and enhanced geothermal reservoirs are the primary applications intended in this study.

It is envisioned that nanoparticles of different sizes, shapes and materials can accompany the fluids injected at one well and can be recovered from another well within the same reservoir. The nanoparticles that made their way to the producing well will be analyzed and correlated with the fracture properties. The recovered particles size distribution

will be related to the size of the fractures. The fracture orientation will be determined from the interwell connection and production history of the nanotracer.

Tailored nanomaterials may have also the ability to record data such as pressure and temperature and register fluid type encountered within the reservoir. These data could be utilized to evaluate in-situ reservoir performance, assess new development plans and determine ways to operate the geothermal system more efficiently.

Nanotracers can be transported into the reservoir rock matrix due to their small physical size. The tracer return curve can then be analyzed to determine the volume of the reservoir. Temperature-sensitive nanotracers can be used to assess the reservoir performance by observing their temperatures behavior deep inside the reservoir far from the wells. Temperature-sensitive nanotracers could be used to provide information on how much heat is removed and how rapidly the heat is replenished.

In order to accomplish the objectives of this study, preliminary experimental testing was conducted to verify the feasibility of transporting particles at nanoscale through a porous medium. This testing was also needed to identify and understand the processes involved in the development of tailored nanosensors and engineering approaches to characterize the fractures. Following that will be the design and fabrication of the nanosensors themselves. Several experiments that imitate the reservoir conditions will then be carried out with these tailored nanoparticles. The results will be used to develop a theory to infer reservoir parameters.

REQUIREMENTS FOR NANOMATERIALS AND CHARACTERIZATION METHODS

Nanoparticles and/or nanowires used in this study and ultimately in the reservoir need to be safe to handle and environmentally friendly. The particles should also be stable in suspension and disperse in solution. Moreover, the interaction affinity of such particles to the reservoir formation should be verified and the particles must not interact with rock matrix (Kanj et al., 2009).

The quantity of the nanotracer produced at the sampling point should be sufficient to be recognizable and at concentrations above the lower detection limit of the devices used to analyze the effluent by at least factor of three. In our experiments, characterization of the nanofluid prior to and after injection was carried out by various techniques. Dynamic Light Scattering (DLS) and Ultraviolet-visible Spectroscopy (UV-visible Spectroscopy) were used to detect the nanoparticles and nanowires, respectively. Scanning Electron Microscopy (SEM) and Optical Microscopy were also utilized to confirm the findings.

Characterization of the rock pore spaces following the injection was required. Studying the nanoparticle or nanowire morphology inside the sample was of equal importance. The objective was to understand the particle size distribution and how they arranged themselves within the porous medium (Kanj et al., 2009). To this end, SEM analyses were performed at different sections of the core samples (i.e. at the inlet, outlet and in the middle).

Nanomaterial Selection

Monodisperse silica particles (silicon oxide, SiO_2) and silver nanowires (AgNW) satisfied all essential requirements and therefore were selected for initial experimentation with nanofluid injection. SiO_2 and AgNW can remain in suspension at different concentrations and particle or wire sizes, and have a narrow band of sizes. SiO_2 has the advantage that it is very similar material to much of the rock itself.

The conditions for the preparation of monodisperse silica particles followed the study done by Bogush et al. (1988). The nanoparticle preparation was accomplished by the hydrolysis of tetraethyl orthosilicate (TEOS) in aqueous ethanol solutions containing ammonia. Initially, particle sizes in the range of 50-130 and 350-390 nanometers were used in the core-flooding and the slim tube experiments, respectively.

The silver nanowires injected had diameters in the range of 50-100 nanometers, and lengths in the range of 5-10 micrometers. The conditions for preparing uniform silver nanowires followed, for the most part, the study by Sun et al. (2002). The formation of silver nanowires is accomplished by reducing silver nitrate ($AgNO_3$) with ethylene glycol (EG) in the presence of silver (Ag) seeds. Polyvinyl pyrrolidone (PVP) is then added to direct the growth of silver into uniform nanowires. The longitudinal and lateral dimensions of the silver nanowires are controlled by changing the reaction conditions. Sun et al. (2002) reported that increasing the reaction temperature resulted in the formation of shorter nanowires. This synthetic method provided uniform nanowires with high yield (mass production) at relatively low temperature.

Nanoparticle Size Determination

The nanoparticle size was chosen based upon the pore size distribution of the core used during

injection. The pore size distribution of the core samples was measured by the mercury (Hg) intrusion method. The intrusion of mercury was performed using the AutoPore IV 9500 Mercury Porosimeter manufactured by Micromeritics. Measurements conducted on the Berea I and II sandstones showed the cores to have pore sizes in the range between 0.01 and 20 micrometers. However, most of the mercury is intruded in the pore sizes of the range of 20 to 300 nanometers. Then, a rule-of-thumb suggested by Kanj et al. (2009) in their copolymer injection into a carbonate core was adopted. This rule-of-thumb was set to avoid two possible phenomena that could affect the permeability of rock; namely, plugging and bridging. The particles should not be too large to plug the pores or too small at high concentration to bridge at the pore entry. Thus, the final size range selected for injection was in the range of 50 to 130 nanometers.Core Characterization Experiments
Preliminary testing of nanofluid injection was carried out using two different cores, Berea I and II. Prior to nanofluid injection, standard experiments to characterize the rock cores were performed, including porosity and permeability measurements. Core sample dimensions, porosity, permeability, pore size distribution and pore volume calculations are summarized in Table 1.

The porosity was measured by mercury intrusion and confirmed by resaturation of the core samples with pure water. The porosity calculation is as follows:

$$\phi = \frac{V_p}{V_B} * 100 \quad (1)$$

$$V_p = W_s - W_d \quad (2)$$

$$V_B = \pi r^2 l \quad (3)$$

where ϕ is the porosity in percentage, V_p and V_B are pore and bulk volumes in cubic centimeter, respectively. W_s and W_d are the weight of core after and before saturation, in gram, respectively. r and l are the radius and length of the core in centimeter, respectively.

These measurements were confirmed by the calculation of the density of Berea I and II sandstones and found to be in good agreement with values reported in the literature (Tayler et al., 1982).

The gas permeability measurement was then measured by introducing nitrogen at different flow rates and inlet pressures. The average gas permeability was found to be around 174 and 131 millidarcy for Berea I and II respectively, by applying Darcy's law for compressible fluids which is given by:

$$k_{gas} = \frac{2\mu p_{out} q_{out} L}{A(p_{in}^2 - p_{out}^2)} \quad (4)$$

where μ is the viscosity in centipoises, q_{tot} is outlet volumetric flow rate in cubic centimeter per second, A is the core cross-sectional area in square centimeter, L is the core length in centimeter and p_{in} and p_{out} are inlet and outlet absolute pressures in atmospheres, respectively.

Table 1: Core characterization data

Property	Measurement	Berea I	Berea II
Core dim's (cm)	Diameter	3.80	3.80
	Length	6.0	5.8
Porosity (%)	Hg intrusion	19.4	19.0
	Resaturation	18.4	18.2
Perm. (md)	Gas perm.	174	131
	App. liq. perm.	85	85
	Liquid perm.	61	94
Size dist. (μm)	Largest pore	20	20
Pore vol. (ml)	By saturation	12.5	12.0

Klinkenberg effect was considered to evaluate the equivalent liquid permeability. According to the Klinkenberg effect, extrapolating the straight line to infinite mean pressure (or zero reciprocal of mean pressure) intersects the permeability axis at a point designated as the equivalent liquid permeability (Amyx et al., 1960). The average equivalent liquid permeability was approximately 85 millidarcy.
The liquid permeability was measured on the same core samples directly. The average liquid permeability was found to be around 61 and 94 millidarcy for Berea I and II respectively. Darcy's law for horizontal flow was utilized to compute the permeability. Darcy's law for horizontal flow is given by:

$$k_{liq} = \frac{q\mu L}{A\Delta p} \quad (5)$$

where q is the volumetric flow rate in milliliter per second, μ is the viscosity in centipoise, L and A are the length and the cross-sectional area of the core in centimeter and square centimeter, respectively. Δp is the differential pressure across the core sample in atmospheres.

SAND-PACKED SLIM TUBE POROSITY AND PERMEABILITY MEASURMENTS

Porosity and permeability measurements as well as pore volume calculations were performed in very similar fashion as outline in the previous section (core characterization experiments). The porosity of the sand was measured by resaturation with pure water and found to be around 35% with pore volume in the order of 52 milliliters. The liquid permeability was also measured and found to be approximately 50 darcy.

NANOFLUID INJECTION EXPERIMENTS

Initial testing with the injection of various nanofluid suspensions was carried out to investigate the viability of transporting nanomaterials through a porous medium. Berea sandstones and sand-packed slim tube were used in the nanofluid injection experiments. The injection process and sampling strategies in all experiments were similar, however, they differed in some aspects such as total pore volume injected, flow rates and sampling frequency.

A schematic of the apparatus is shown in Figure 1. Nanofluid solution was contained in a pressure vessel downstream of the water pump. The nanofluid was injected into the core and/or slim tube with the aid of nitrogen pressure. The configuration also allowed for injection of particle-free water, without interrupting the flow.

Prior to the injection of the nanofluids, the cores as well as the slim tube were preflushed with pure water to displace rock fines and debris. The nanofluid injection sequence was similar to the process described by Kanj et al. (2009). The sequence involved the injection of a pore volume of nanofluid followed by a continuous injection of pure water. The pore volume was determined as outlined earlier in the description of the porosity calculations. In particular, two pore volumes plus the dead volume (the volume of the tubes and fittings) were injected. The dead volume was required to fill the tubes completely prior to nanofluid entering the core. Following that was the first pore volume of injected fluid which should completely fill the pore spaces. The second pore volume was used to confirm the filling. The pore volumes for all cores are reported in Table 1. In the slim tube experiment, the nanofluid injected is only 25% of the pore volume plus dead volume .
The pore, dead and injected volumes were computed as follows:

$$V_p = V_B \phi \tag{6}$$

$$V_d = \pi r_t^2 l_t \tag{7}$$

$$V_{inj} = 2V_p + V_d \tag{8}$$

where r_t and l_t are the radius and length of the tube in centimeter, respectively. V_d and V_{inj} are the dead and total injected volumes in cubic centimeter, respectively. The rest of parameters have their usual definition.

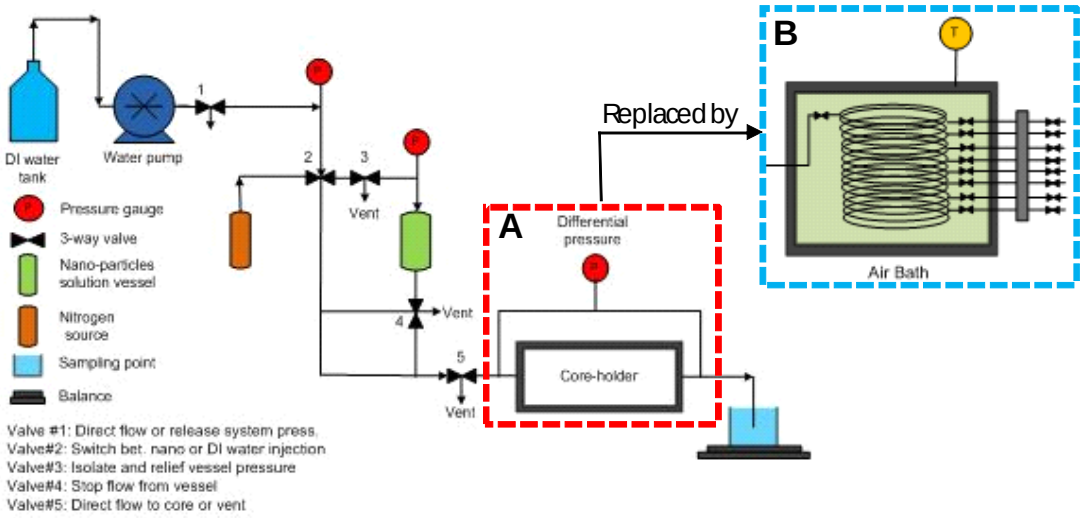

Figure 1: Experimental apparatus for nanofluid injection into (A) core samples and (B) sand-packed slim tube.

Subsequent to the injection of the nanofluid (pore and dead volumes), a continuous flow of pure water (post injection) was introduced. Depending on the experiment, several pore volumes of pure water were injected while the effluent samples were collected. The total time of the experiment, flow rates and frequency of sampling were also experiment dependent. For instance, the total time of the Berea I injection experiment was approximately 2 hours. The injection was at the rate of one milliliter per minute at low differential pressure.

Sampling immediately following the injection was very frequent. As time progressed, the sampling frequency was lowered. There was no harm in taking samples more frequently than necessary since time required to collect the samples was not an issue. Not all these samples needed to be analyzed. The infrequent samples had indicated the trend of the returning nanoparticles and more details (if needed) could still be obtained by analyzing the samples in between. If the samples had not been taken frequently enough, there would be no way to recover the results without repeating the experiment.

RESULTS

This section provides the results of the initial nanofluid injection experiments conducted on Berea core samples as well as sand packed slim tube with different nanofluid suspensions. Generally, the objective of the experiment, the characterizations of the original nanofluid injected, effluent samples collected and cross-sections of the rock matrix are presented. Hypotheses made with relation to the experiment objective are also emphasized and verified as applicable.

Berea I silicon oxide suspension injection results

The main objective of this experiment was to achieve a proof of concept on the use of nanoparticles as tracers to characterize fractured reservoirs. Silicon oxide (SiO_2) nanoparticles were flowed successfully through the Berea I sandstone core. The injected nanoparticles were transported through the pore spaces of the rock and were detected in the effluent. The recovery of the nanoparticles following their injection was verified. It has been demonstrated that they were not trapped in the pore spaces by hydraulic, chemical or electrostatic effects. The SiO_2 nanoparticles had a relatively narrow distribution of sizes between 50-130 nanometers (Figure 2). The nanoparticles were easily distinguishable from the core fines and debris due to their size and spherical shape, even though all were made of same material as the rock itself (silica).

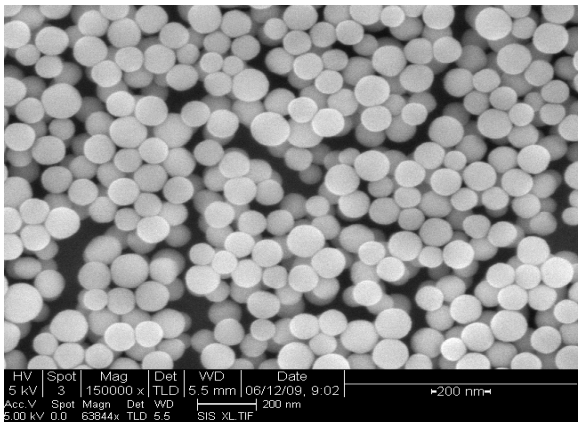

Figure 2: SiO_2 nanospheres in the injected nanofluid, image obtained by SEM.

The effluent samples were examined qualitatively for the existence of the nanoparticles using the DLS technique. For instance, an effluent sample at later post injected pore volume showed a particle size distribution as depicted in Figure 3.

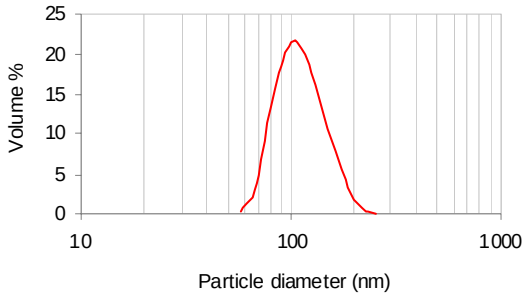

Figure 3: Particle size distribution by volume percentage of an effluent sample at later post injected pore volume.

The more precise approach using SEM imaging of the effluent confirmed this finding (Figure 4). The average nanoparticle size in Figure 4 was around 100 nanometers.

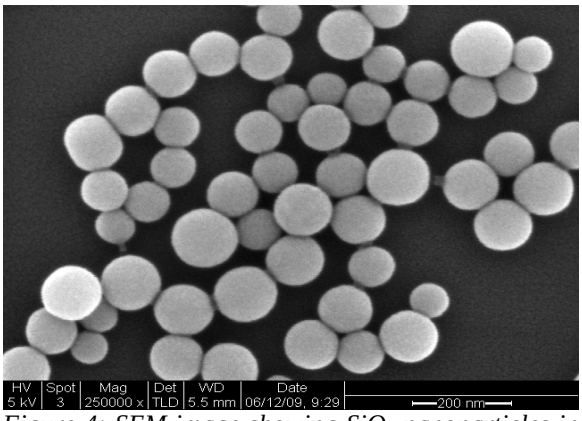

Figure 4: SEM image showing SiO_2 nanoparticles in the effluent.

It is worth mentioning that some particles larger than those injected were detected by DLS in some of the early effluent samples. An example of the size distribution based on the volume percentage of particles is illustrated in Figure 5. It was believed that these larger particles were core fines which were produced from within the rock pore spaces.

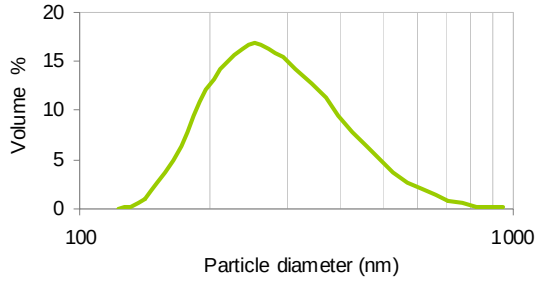

Figure 5: Particle size distribution by volume percentage of effluent sample containing core fines and debris.

To verify this hypothesis, SEM images of the same sample were taken as shown in Figure 6. The presence of such fines has resulted in the size distribution estimated by light scattering technique shown in Figure 5.

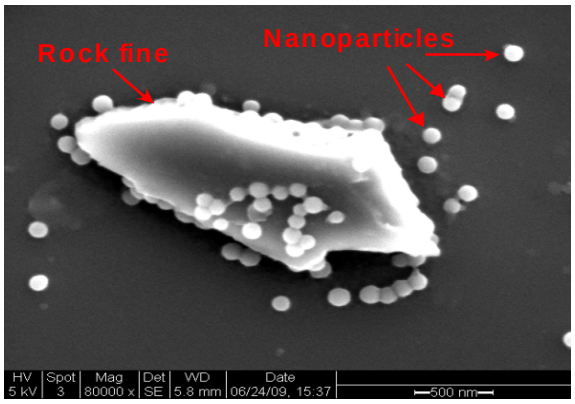

Figure 6: SEM image of rock fine relative to injected nanoparticles.

These larger particles were detected right after the injection of the two pore volumes of nanofluid plus the dead volume of the tubes. Traces of these particles have been detected within the first injected pore volume of pure water (post injection of pure water) with a decreasing trend as depicted in Figure 7. The larger particles were only produced in the early part of the injection. In Figure 7, each particle size was plotted individually, showing its volume percentage as function of cumulative pore volumes injected. Recall that the pore volume of this core was approximately 12.5 milliliters. It can be concluded that these larger size fines and debris have been produced and that the core's pore spaces had been washed out during the injection process.

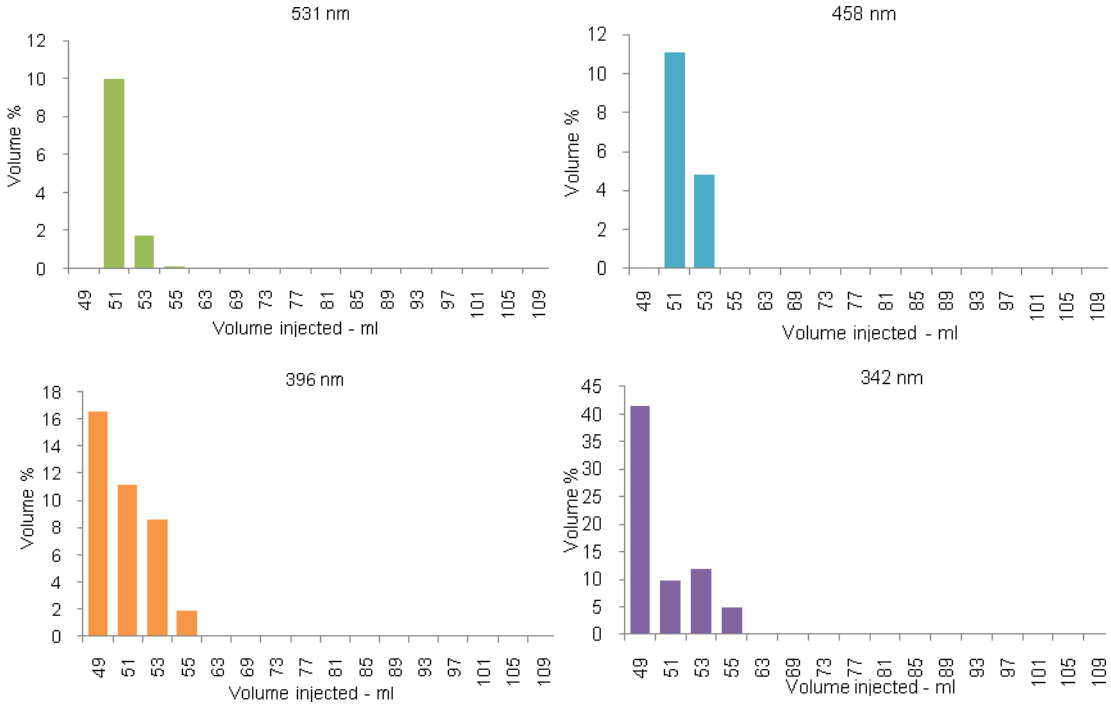

Figure 7: Large particles (core fines and debris) as function of cumulative pore volumes injected.

Based on the pore size distribution measured by mercury intrusion (0.01 to 20 micrometers), the nanoparticles should be able to pass through the core. This hypothesis was confirmed in Figure 8 by generating similar plots as in Figure 7 for a particle size within the range of the injected SiO_2 nanoparticles (50-130 nanometers). Smaller particles were not detected by DLS at earlier post-injected pore volumes because larger particles acted as a shadow over smaller ones and therefore they were not visible by DLS. Smaller nanoparticles were produced constantly in all pore volumes throughout the injection. It has been observed, however, that the continuous injection of pure water was not enough to show the peak of tracer concentration as function of injected volumes or time, probably because of the high concentration of nanofluid and/or quantity injected. Nanoparticles continued to be produced from the core until the end of the injection.

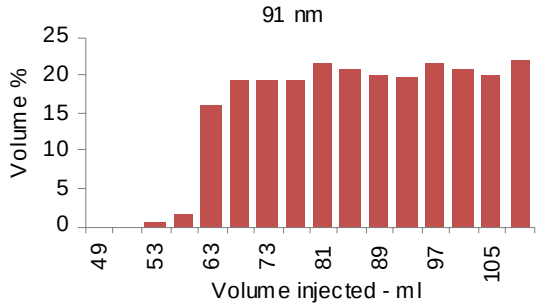

Figure 8: SiO_2 nanoparticles volume percentage as function of cumulative pore volumes injected.

The production history of injected nanoparticles was illustrated better by plotting their volume percentage as it varied with time (Figure 9). It was expected that the concentration of each nanoparticle should decrease as more pore volumes of pure water were injected. It was evident from the production history plots that there should have been more post injection of pure water to be able to detect each particle maximum concentration peak.

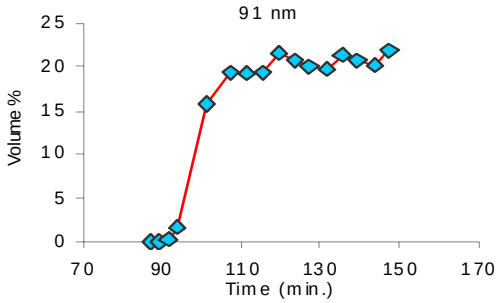

Figure 9: Production history of nanoparticle of size 91 nanometers.

Subsequent to the analysis of the effluent, the interior of the rock itself was examined by cutting the core into slices. Specifically, middle and outlet slices (Figure 10) were examined most closely because nanoparticles present in those sections had clearly passed the inlet.

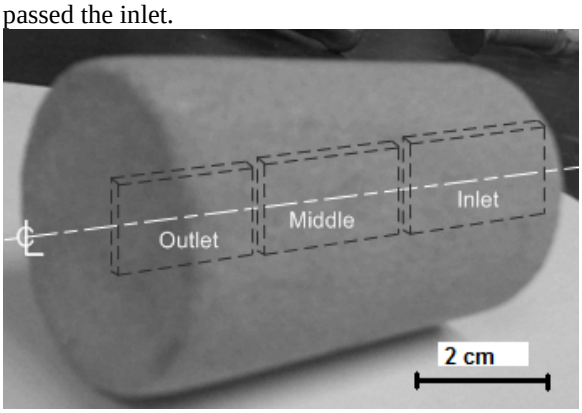

Figure 10: Rock sections for SEM analyses.

Figure 11 shows an SEM image of the pore spaces at the middle section of the core. The SiO_2 nanoparticles are visible as little white spheres. These spheres were approximately 100 nanometers in diameter. This demonstrated unambiguously that the nanoparticles had been transported through the pore network of the reservoir rock.

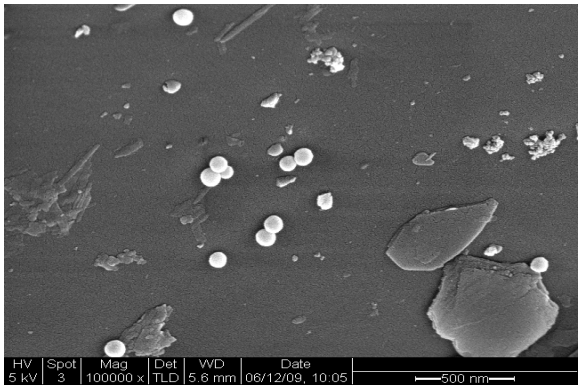

Figure 11: Nanoparticles at the middle section of the rock. Non-spherical objects are the natural fines and debris from the rock itself.

In terms of characterizing the fractures in the rock, which is one primary objective of the project, these preliminary experiments showed promise. Figure 12 shows that the nanoparticles passed through pores of sizes larger than themselves, but were unable to pass into the tinier natural fracture that existed within the rock structure. A slightly smaller nanoparticle could have entered the fracture.

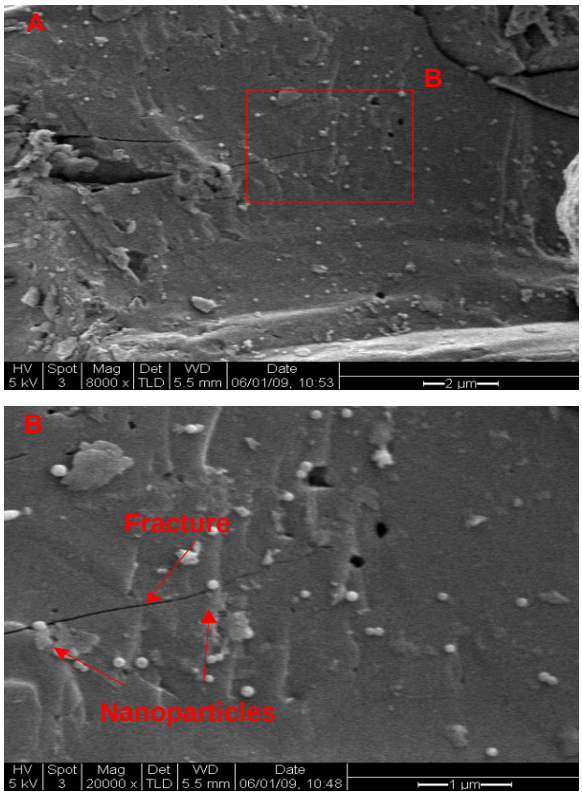

Figure 12: (A) Natural fracture with two nanoparticles at its entry, (B) close-up image.

Clearly, this experiment served its objective in proving that nanoparticles had been transported within the rock pore matrix.

Sand-packed slim tube silicon oxide suspension injection results

A second experiment was conducted using different flow apparatus, a 10 meter long sand-packed slim tube, to study the transport and recovery of injected SiO_2 nanoparticles through a longer flow path. This experiment imitates near field interwell distance as in the conventional interwell tracer test. The silicon oxide nanoparticles were detected at the effluent confirming their transport (Figure 13). The permeability was unaltered during and after the injection of the nanofluid.

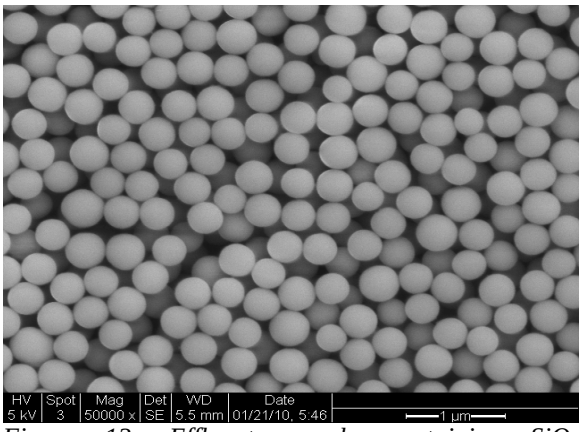

Figure 13: Effluent sample containing SiO_2 nanoparticles.

The SiO_2 nanoparticles injected had an average particle size of approximately 350 nanometers as demonstrated in Figures 14 and 15 by light scattering and scanning electron microscopy, respectively.

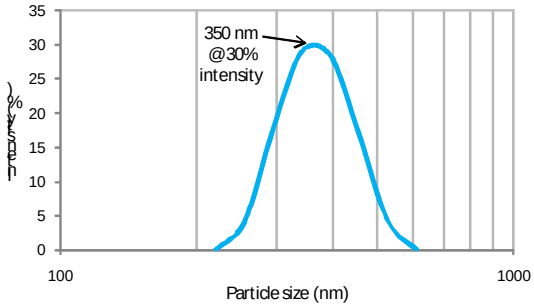

Figure 14: Particle size distribution by light intensity percentage of the influent injected.

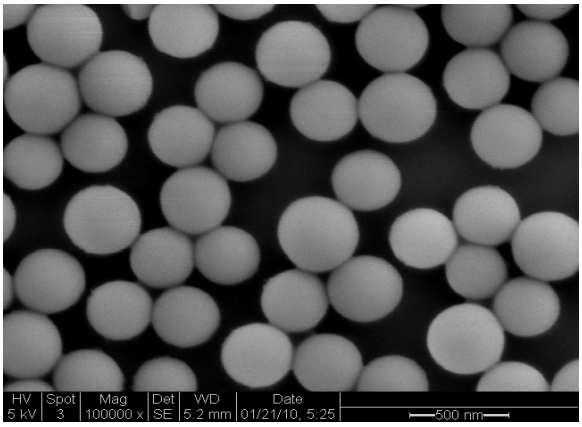

Figure 15: Monodisperse SiO2 nanospheres of the influent with an average size of 350 nm.

Based on the light scattering measurements, the intensity of the incident light should remain unchanged for every particles size regardless of the sample concentration. In this case, the intensity of around 30% was measured at particle size of 350 nanometers of the original nanofluid injected (Figure

14). Therefore, effluent samples collected during post injection of pure water that contain any nanoparticle concentrations within the detection limits of instrument used, should have the same intensity for that particular particle size. The light intensity of effluent samples is plotted against post injected pore volumes (PVI) as illustrated in Figure 16.

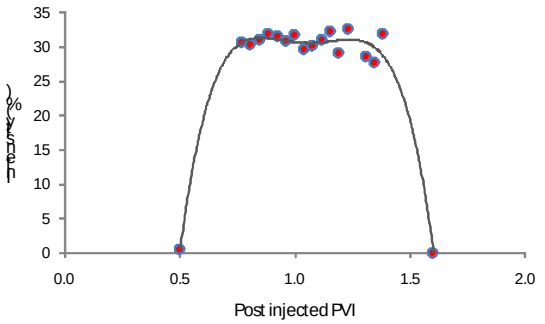

Figure 16: Intensity measurements of effluent samples.

It is evident from above graph that the nanoparticles exist in the effluent samples with same intensity of the original silicon oxide nanofluid influent (i.e. 30%) as depicted in Figure 14. The nanoparticles were identified following the post injection of about half pore volume of pure water and produced continuously until displaced through the second pore volume. The increasing content of nanoparticles within that pore volume can be observed visually as shown in Figure 17. Cloudy samples are characterized by being highly concentrated with SiO_2 nanoparticles as oppose to semi-transparent samples.

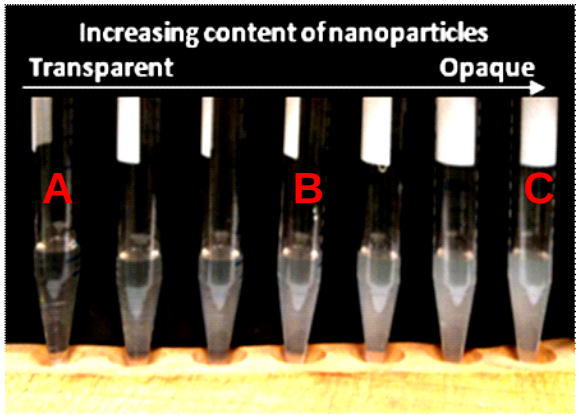

Figure 17: Visual characterization of effluent samples for their SiO_2 nanoparticles content based on color.

Scanning electron imaging has confirmed the variation in the particle concentrations. A series of SEM images (Figure 18) were taken for samples A, B and C of Figure 17. These images show the difference in particle count or concentration clearly. Note that the volume of each sample was identical and micrographs were taken at the same magnification.

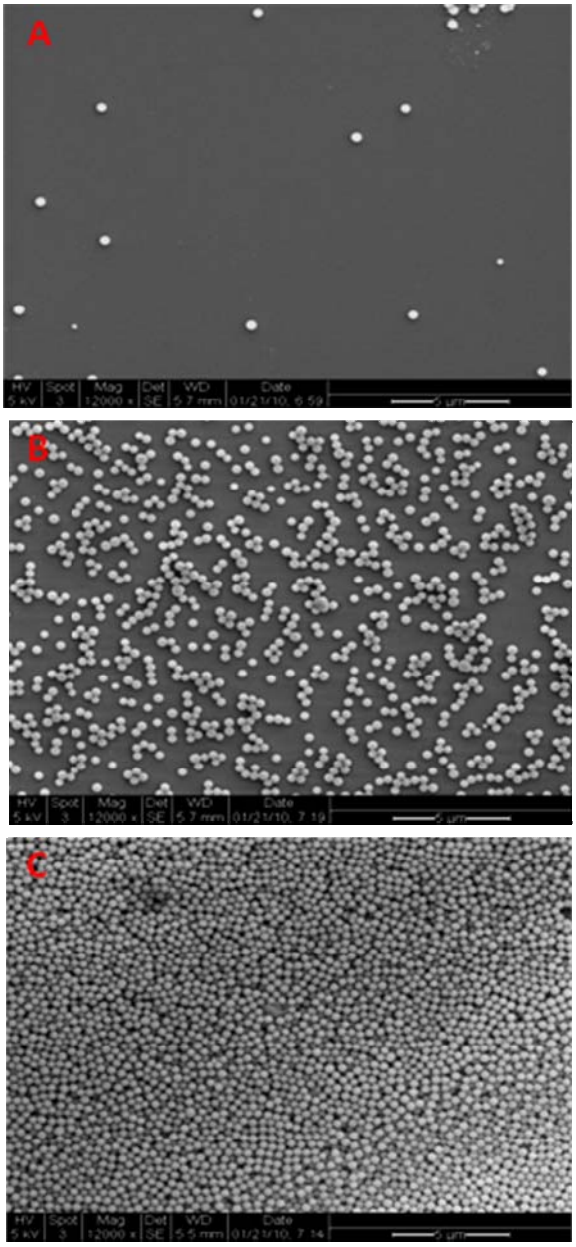

Figure 18: SEM images at sample A, B and C of Figure 17.

Thus, it has been demonstrated that the spherically shaped nanoparticles can be recovered following their injection not only through short core plugs but also through a long flow path without being trapped within the flow conduits.

Berea II silver nanowires suspension injection results

A third experiment was carried out using wire-like nanoparticles. Silver nanowires were injected through the Berea sandstone core. The objective of this

experiment was to investigate the feasibility of transporting nanowires in the tortuous pore network of typical reservoir formation rock.

Silver nanowires were injected through the Berea II sandstone core, however were not detected in the effluent. They were found to be trapped at the inlet section of the core within the pore network. Figure 19 is an SEM image of the front face of a 3 millimeter slice cut at the inlet section of the core (Figure20).

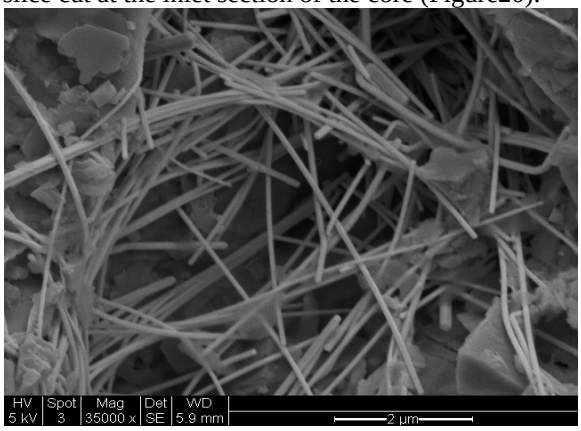

Figure19: Silver nanowires trapped in the pore network of Berea II sandstone.

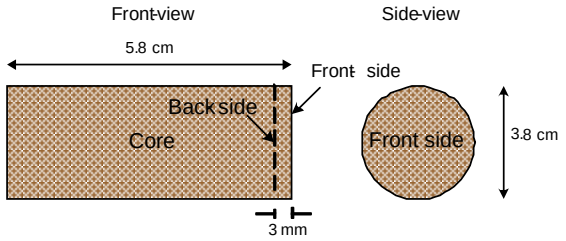

Figure 20: Front and side view sketch of Berea sandstone with slice position and dimensions.

The effluent samples were analyzed and/or characterized using UV-visible spectrophotometry and optical imaging. The silver nanowires injected had an optical signature (UV-visible spectra) very similar to typical silver nanowires reported in the literature (Sun et al., 2001) as depicted in Figure21. The size of injected nanowires was 50-100 nanometers in diameter, and 5-10 micrometers in length.

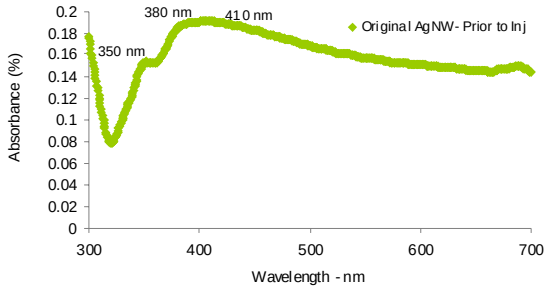

Figure21: UV-visible spectra of injected silver nanowires.

The size of original silver nanowires was further confirmed by optical microscopy imaging. Figure 22 is an optical image of the injected nanowires. As mentioned earlier, more accurate measurements of sizes may be obtained by Scanning Electron Microscopy.

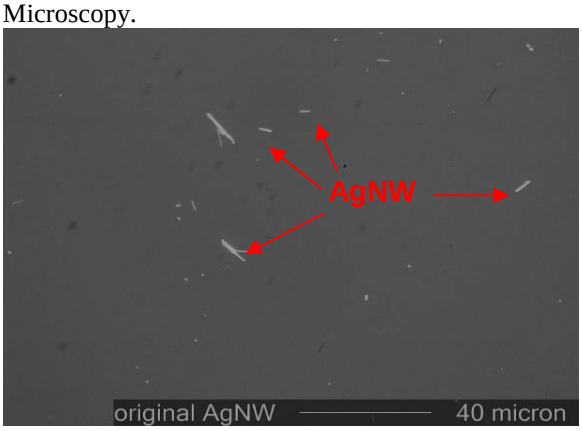

Figure22: Optical image of the original silver nanowires suspension.

The effluent samples were examined for the existence of the nanowires. Among the 139 samples collected, several samples were strategically selected. Initially, the analysis was performed on six samples. One sample from the pore volume collected during the injection of the nanofluid and others from subsequent injection (post injection of pure water) of first, second, third, sixth and thirteenth pore volumes. The UV-visible spectra of these samples were taken as depicted in Figure23.

The spectra of all effluent samples exhibited the behavior of pure water, with no sign of silver nanowires, as opposed to the originally injected nanofluid (red-curve). This finding was verified by optical microscopy imaging shown in Figure24. The black traces in the images were just dust.

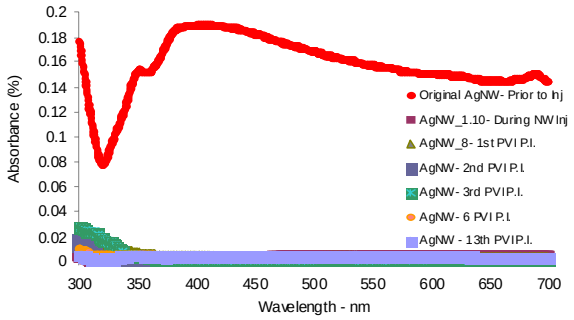

Figure23: UV-visible spectra of selected effluent samples.

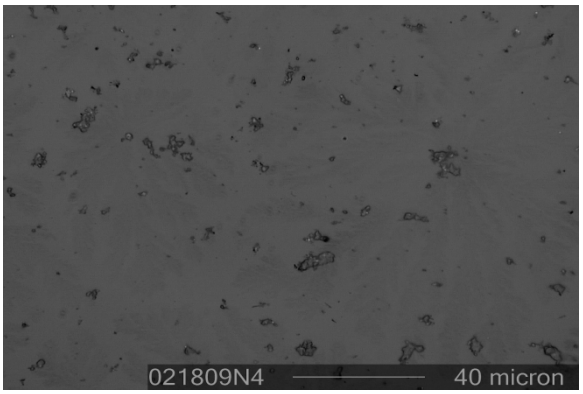

Figure24: Optical image of effluent sample at the second post injected pore volumes.

Based on these findings, it was decided to not analyze either the samples in between or samples from later pore volumes but rather focus our investigation on the causes that prevented the nanowires from being transported through the pore spaces. The aggregation of the silver nanowires or simply their geometry may have imposed a flow constraint. It is known that silver nanowires are best dispersed in ethanol solution. Since the silver nanowires were diluted in water before and after injection, it was suspected that they have aggregated at injection and hence plugged the fluid passages right at the inlet section. The permeability was measured during each sample collected and plotted against the cumulative injection as illustrated in Figure25.

There was a drop in the permeability from approximately 94 to 51 millidarcy, or about 45% reduction. This drop began during the injection of the nanofluid and stabilized through the post injection of the fifth pore volume. This result also supported the inference that some of the pore spaces (especially at the inlet section) had been plugged by the silver nanowires. The core was back-flushed by the injection of 11 pore volumes of pure water. The UV-visible spectra of representative samples of every pore volume injected were measured. All showed the behavior of pure water, similar to that depicted earlier in Figure23, indicating that the nanowires remained in the core and were not backflushed out.

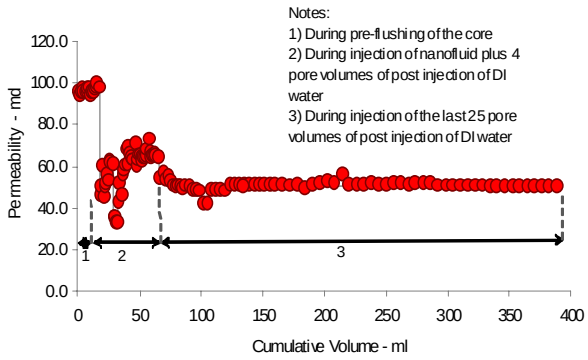

Figure25: Permeability measurement verses cumulative volume injected.

The gas permeability was remeasured to assess the effect of the nanowires on the core after removing the few millimeters slice from the inlet side. The core was prepared by drying it in the furnace at 160˚F for 24 hours. The gas permeability was repeated at exactly the same flow rates in the earlier gas permeability measurement prior to injection of the silver nanowires. Figure 26 is a comparison between both measurements. The change was minimal -- about 2.7 % difference.

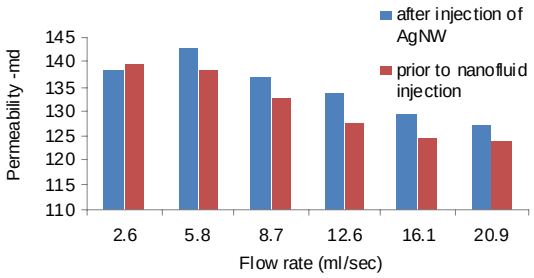

Figure26: Gas permeability comparison before and after cutting the slice at the inlet.

The original gas and equivalent liquid permeabilities were restored by cutting off a slice of core at the inlet. Therefore, it was demonstrated that all the nanowires had been trapped within the removed slice. SEM imaging has confirmed this unambiguously. The analysis was performed on the front and back sides (Figure20) of the slice. Figure 27 and 28 are SEM images of the front and back sides, respectively. The silver nanowires were clearly trapped at the front side while the back side was free of nanowires. This demonstrated that the nanowires could not pass through the pores of the core even for a couple of millimeters. The experimentation with silver nanowires is still ongoing. A trial injection of shorter nanowires (less than 1 micron) will be conducted to

verify if their geometry has imposed constraint on their transportation through the core.

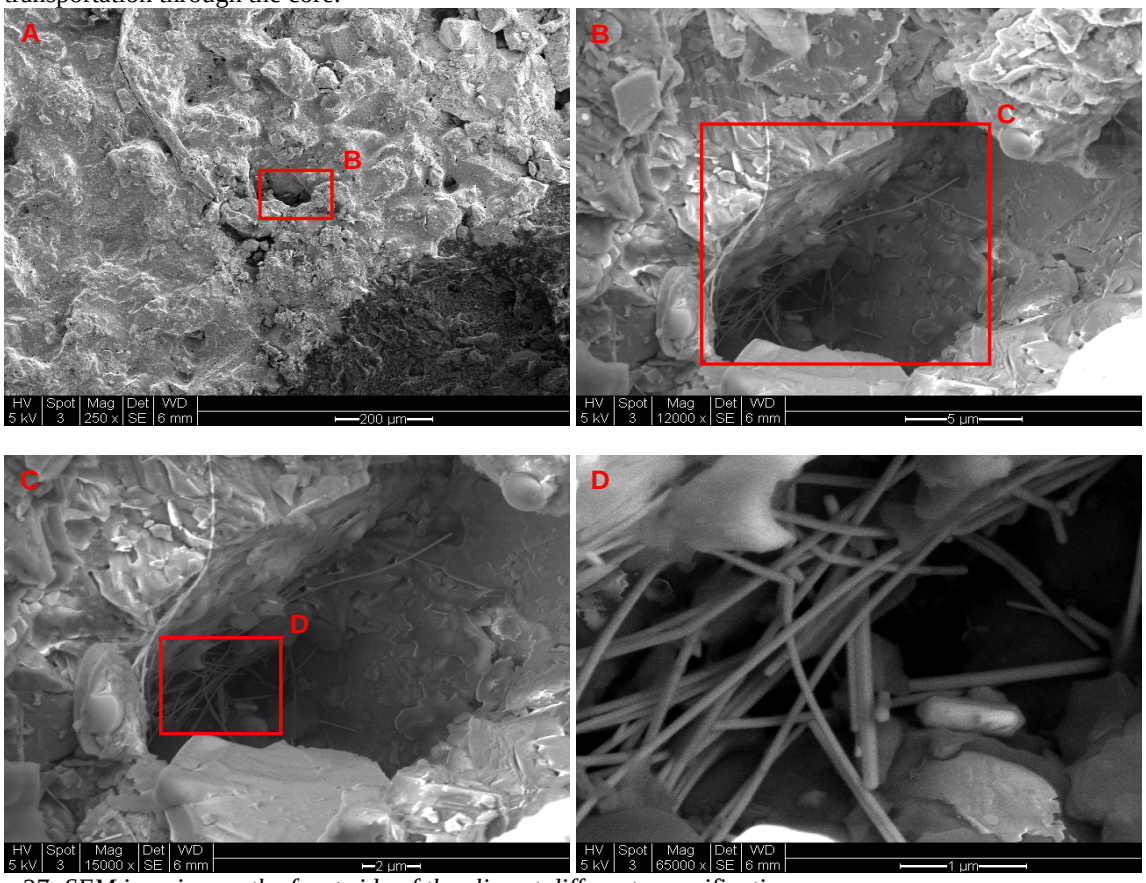

Figure27: SEM imaging on the front side of the slice at different magnifications.

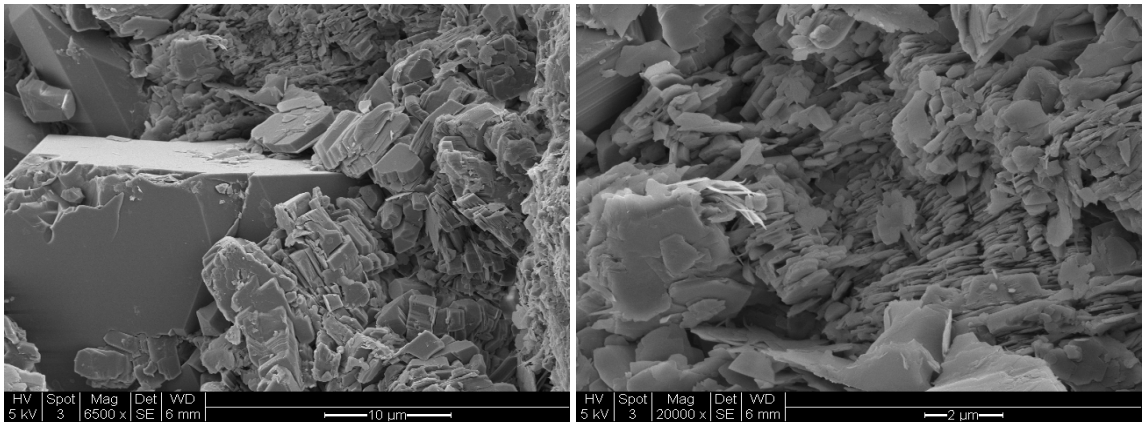

Figure28: SEM imaging on the back side of the slice.

CONCLUSION

Extracting more energy is the primary goal of all energy producing entities. One way to achieve this goal is by obtaining more detailed information about formations thousands of feet below the earth's surface. Breakthroughs in nanotechnology offer alternatives for reservoir monitoring and analysis technologies that are more efficient, environmentally sound and capable of providing information that is not readily accessible with current technologies.

In order to investigate the feasibility of utilizing nanosensors in illuminating reservoir properties in general and fracture network properties in particular, it was essential to verify their transport mechanism through typical formation rock core samples. Initial testing with nanoparticles was also required to

develop the understanding of their optimum injection procedures, sampling strategies and characterization techniques. Accordingly, various laboratory-scaled core-flooding experiments with inert nanoparticle and nanowire suspensions were conducted.

The spherical silicon oxide nanoparticles were transported readily through a representative Berea sandstone core sample as well as 10 meter sand-packed slim tube. The nanoparticles were identified in the effluent samples as well as within the pore spaces themselves. The silver nanowires, however, were trapped at the inlet of the core and therefore could not be flowed through.

ACKNOWLEDGEMENTS

The authors wish to thank Robert Jones, Sirion SEM Laboratory Manager, for his support in this project. The authors also acknowledge the continued support of the Department of Energy (under contract number DE-FG36-08GO18192).

REFERENCES

Amyx, J. W., Bass, D. M. Jr., and Whiting, R. L. (1960), Petroleum Reservoir Engineering, Physical Properties. McGraw-Hill Book Co.

Bogush, G. H., Tracy, M. A., and Zukoski, C. F., IV: "Preparation of Monodisperse Silica Particles: Control of Size and Mass Fraction," Non-Cryst. Solids **104** (1988) 95.

Kanj, M., Funk, J., and Al-Yousif, Z.: "Nanofluid Coreflood Experiments in the Arab-D," SPE paper 126161, presented at the 2009 SPE Saudi Arabia Technical Symposium and Exhibition held in Saudi Arabia, Alkhobar, May 09-11.

Sun, Yugang, Yin, Yadong, Mayers, Brian T., Herricks, Thurston and Xia, Younan: "Uniform Silver Nanowires Synthesis by Reducing $AgNO_3$ with Ethylene Glycol in the Presence of Seeds and Poly (Vinyl Pyrrolidone)," American Chemical Society 2002.

Taylor, R.E., Shoemaker, R.L. and Groot, H.: "Thermophysical Properties of Selected Rocks," A Report to U.S. Geological Survey. TPRL 271 32 pp., Thermophysical Prop. Res. Lab., Purdue Univ., Ind., 1982.